Scanning tunneling microscope investigation of local density of states in Al-doped ZnO thin films

Edward M. Likovich, Rafael Jaramillo,* Kasey J. Russell, Shriram Ramanathan, and Venkatesh Narayanamurti
School of Engineering and Applied Sciences, Harvard University, Cambridge, Massachusetts 02138, USA
(Received 17 May 2010; revised manuscript received 7 January 2011; published 24 February 2011)

The electrical properties of grain boundaries in technologically relevant oxide thin films are the subject of both applied and fundamental research. Here we present an investigation of the local density of states (LDOS) in sputtered Al-doped ZnO using a scanning tunneling microscope. We observe a pronounced difference in the tunneling conductivity recorded on- and off-grain, with the grain boundary LDOS peaked ∼600 meV below the Fermi level. This provides a direct measurement of the distribution of charge traps that is of relevance in advancing understanding of carrier conduction in this transparent conducting oxide.

DOI: 10.1103/PhysRevB.83.075430 PACS number(s): 77.55.hf, 68.37.Ef, 73.20.−r, 61.72.Mm

I. INTRODUCTION

Aluminum-doped zinc oxide (AZO) is an important material for incorporation into optoelectronic devices, primarily as transparent electrodes in thin film solar cells, UV photodetectors, and UV light emitters.[1] AZO exhibits similar electronic properties to ZnO: a wide optical band gap ($E_g \geqslant 3.37$ eV), a strong exciton binding energy (60 meV), and optical transparency throughout the visible spectrum.[2–4] Doping ZnO with Al increases the electrical conductivity by several orders of magnitude and the material is called a transparent conducting oxide (TCO). AZO is second only to indium tin oxide (ITO) in present-day utilization, and both materials have seen a surge of research interest as the scale and scope of applications for TCO materials has grown in recent years.[5–11]

The fabrication of AZO films has been well documented for a variety of methods including chemical vapor deposition,[12] sputtering,[5,6] and pulsed laser deposition.[7] In general, the electrical properties of grain boundaries continue to attract much interest,[13,14] and significant efforts have been undertaken to understand and control the formation of grains in AZO films, since grain boundaries are known to host imperfections such as segregated Al or Al_2O_3 clusters.[8,9] A recent study of temperature dependent electronic transport in AZO films confirms that grain boundary scattering can have a significant effect on electron transport.[10] However, the details of the electronic structure responsible for this phenomenon are still understood only qualitatively, as a direct (model-independent) measurement of the number and distribution of charge traps at grain boundaries has not yet been reported. Here we present a study of local electron spectroscopy in sputtered AZO films using a scanning tunneling microscope (STM). STM operation is based on vacuum tunneling, which allows us to probe bias-dependent differential conductivity as a function of spatial position.[15–17] From this measurement, we can compare the on-grain and grain boundary local density of states (LDOS) as a function of energy.

II. EXPERIMENTAL METHODS AND RESULTS

Our ZnO:Al thin films were grown on c-plane sapphire by RF magnetron sputtering from a Zn:Al 1.2 wt. percent target (99.99%, ACI Alloys, Inc.). The RF power, substrate heater temperature, Ar flow rate, O_2 flow rate, and total process pressure were 100 W, 200 °C, 40 sccm, 6.4 sccm, and 2.5 mTorr, respectively. An atomic force microscopy (AFM) image of a surface patch is shown in Fig. 1(a) and displays granular structure. In Fig. 1(b) we show the optical transmission (T) and absorption (A) spectra of this AZO film which exhibits low absorption over the wavelength range $\lambda = 400$–1100 nm relevant to many applications. The optical bandgap $E_g = 3.89 \pm 0.04$ eV is determined from $A(\lambda)$ as described in Ref. 18.

The as-grown films were loaded into a home-built STM. Measurements consisted of grounding the etched tungsten tip and applying bias to the AZO film, such that positive bias corresponds to electron injection from the tip to the sample (vice versa for negative bias). All measurements were conducted at room temperature and $\sim 10^{-8}$ torr.

Tunneling topography $z(x,y)$ was measured for a variety of fixed sample biases by rastering the tip across the sample surface and adjusting z to maintain constant tunneling current. Here z describes the motion of the tip along the direction perpendicular to the sample plane. The tunneling current I is given by[19,20]

$$I(V) = \frac{2\pi e}{\hbar}\left(\frac{\hbar^2}{2m}\right)^2 \int_0^{eV} T(S,\phi,E,V)\rho_s(E)\rho_t(E-eV)\,dE, \tag{1}$$

where $\rho_s(E)$ is the local density of states in the sample and $\rho_t(E)$ is the local density of states in the tip. $T(S,\phi,E,V)$ is the 1D WKB tunneling matrix element which depends on tip-sample separation S, the tunneling potential barrier height ϕ, the electron energy E measured from the sample Fermi level, and the applied bias V. If ϕ and ρ_s were to not vary across the sample (i.e., had no x-y dependence), then $z(x,y)$ would be adjusted to maintain constant S and would simply reflect the surface topography of the sample. Conversely, if the sample were perfectly flat but had a laterally-varying LDOS and/or ϕ, then z would be adjusted so that the changes in LDOS and ϕ would be compensated by changes in S to maintain constant current. In the most general case the topography, LDOS, and ϕ can vary across the sample, and the measured $z(x,y)$ reflects a convolution of these parameters. For example, the STM tip will retract (extend) to maintain a constant tunneling current for both higher (lower) physical features, and greater (lower) LDOS. By scanning over the same sample area for varying biases, we can gain insight into relative LDOS as a function of bias by observing how the topographic features

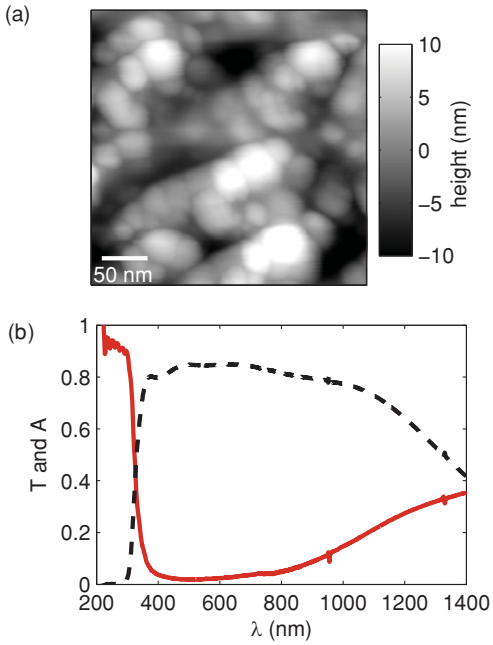

FIG. 1. (Color online) Surface topography and optical absorption of the sputtered AZO film. (a) AFM topography map of the as-deposited film, acquired with a sharp tapping mode probe (Nanosensors SSS-NCHR). Grains are approximately 10–50 nm in lateral size. Surface roughness analyzed on 40×40 nm^2 patches is 0.7 ± 0.2 nm rms. (b) Optical transmission (T, dashed black line) and absorption (A, solid red line) spectra. Data are measured on a Hitachi U-4001 spectrophotometer with an integrating sphere, and the sample is grown on a 0.5 mm thick sapphire substrate. The film is transparent in an optical window from the bandgap in the UV to the plasma absorption in the IR.

change. The variation in ϕ across sputtered AZO films has been independently measured using Kelvin force microscopy, and the difference between grains and grain boundaries was found to be no more than 100 meV. Variations of this scale have negligible effect on our analysis, indicating that variations in our measured $z(x,y)$ data are purely a function of surface topography and variations in LDOS.

Figure 2 shows tip-sample separation scans $z(x,y)$ of the same area taken at -0.9 V and -0.1 V sample bias. The relative contrast between grains and grain boundaries changes slightly with bias, suggesting that the relative LDOS varies in energy. The rms roughness is $\sim 30\%$ larger than that measured with the AFM, which is consistent with a contrast between the LDOS on grains and grain boundaries. The significantly sharper STM tip also undoubtedly contributes to the larger granular relief measured in the STM. The higher resolution of the STM compared to AFM also affects the apparent lateral size of the individual grains, with the STM images showing grains on the scale of 10 nm much more clearly than the AFM image.

We are most interested in the dependence of LDOS on film granularity. To probe this, we pause the tip such that it is positioned over either a grain or a grain boundary, and sweep the bias while recording tunneling current. We also monitor a lock-in amplifier that applies a 36 mV ac modulation to the sample bias and records the variation in tunneling current. Thus

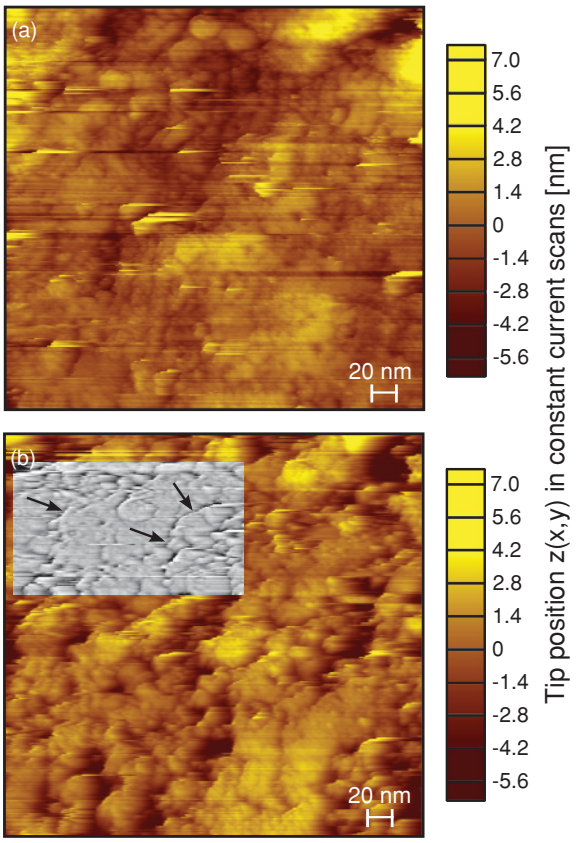

FIG. 2. (Color online) STM constant current topography maps of the same area taken with (a) -0.9 V and (b) -0.1 V bias applied to the sample relative to the tip. In the inset region of (b), the data have been high-pass filtered to emphasize sharp features; prominent grain boundaries are identified with arrows. Positive height corresponds to the tip retracting from the sample, negative height corresponds to the tip extending toward the sample. Line errors result from electrical and mechanical noise that disrupts the STM feedback loop. The rms surface roughness analyzed on 40×40 nm^2 patches is 0.9 ± 0.3 nm and 1.3 ± 0.4 nm for (a) and (b), respectively.

we are able to concurrently monitor I and $\frac{dI}{dV}$ as a function of bias V. In these I–V sweeps we do not observe a zero conductance region characteristic of a semiconductor bandgap, which confirms that the sample is degenerately n-type doped, as expected from the Al doping.

In Fig. 3 we show $\frac{dI}{dV}$ data recorded on grains and grain boundaries. In both cases the plotted curves are the average of data measured at multiple locations on the sample. The on-grain conductivity is typical for tunneling between two metals and is nearly featureless. In contrast, the grain-boundary data is non-monotonic with prominent local maxima. Although interpreting differential tunneling conductivity is notoriously difficult (see Sec. III), the comparison between grain and grain-boundary $\frac{dI}{dV}$ data shown in Fig. 3 clearly implies a peak in the grain boundary LDOS located $\sim$0.6 eV below the Fermi level. Being so close to the conduction band edge, these states are naturally identified as charge traps. We emphasize that the data in Fig. 3 were recorded on the same sample with the same tungsten tip, and with grain and grain-boundary scans interspersed to control for any systematic changes in the tip or the tunneling conditions. The difference between the grain and

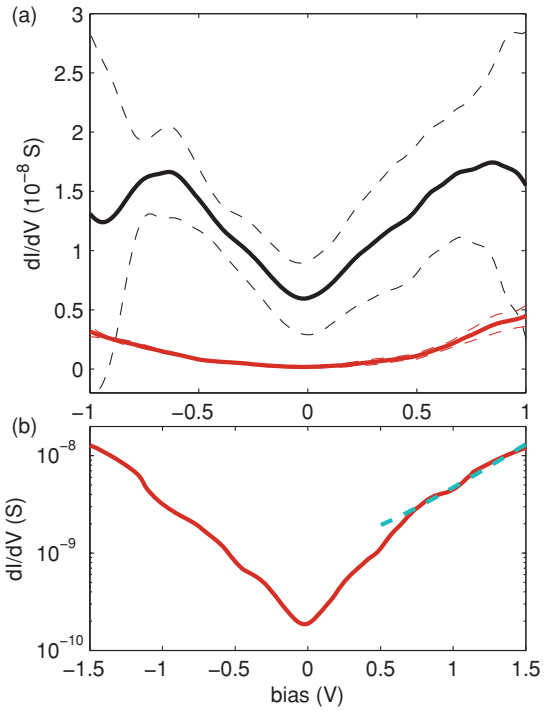

FIG. 3. (Color online) Measured differential tunneling conductivity. (a) $\frac{dI}{dV}$ measured on grains (red) and grain boundaries (black). On-grain curve is the average of 148 scans measured at three different locations on the sample; grain-boundary curve is the average of 132 scans measured at four different locations. The standard deviations of these scans are indicated by the thin dashed lines bounding the averages. All scans were recorded on the same sample with the same tungsten tip, and with the grain and grain-boundary scans interspersed. (b) $\frac{dI}{dV}$ measured on-grain to higher bias in order to fit for the tunneling parameters (see Sec. III); the teal dashed line shows the fit for $V > 0.5$.

grain-boundary data sets therefore represents real variation in LDOS across the sample. It is important to note that the free surface of a grain is itself a grain boundary, and therefore it warrants asking what difference other than topography might be expected between exposed grains and grain boundaries; this is a general concern for all scanning probe studies of granular materials. The free surface of a grain represents a kinetic steady state between crystalline ZnO:Al and the environment (be it vacuum or air), while the exposed grain boundary represents a steady state between the environment and the intergranular material. This intergranular material may exhibit different stoichiometry and coordination from the crystalline bulk, and therefore it is also expected that the exposed grain boundary could have different electronic structure. Nevertheless, our observation of such different spectroscopy on grains and grain boundaries is by itself an interesting result that supports the distinction between these two types of exposed material.

III. DATA ANALYSIS AND DISCUSSION

Although much work has been done to establish the theory of vacuum tunneling,[16,17] extracting even qualitative LDOS from tunneling data remains a daunting task that is complicated by a number of factors that are difficult to control. These factors can be conceptually divided into two categories, the tip density of states and the tunneling conditions. The effects of these factors on the measured $\frac{dI}{dV}$ data are clearly visible in the derivative of Eq. (1):

$$\frac{dI(V)}{dV} = \frac{2\pi e}{\hbar}\left(\frac{\hbar^2}{2m}\right)^2\Bigg[T(S,\phi,E=eV,V)\rho_s(eV)\rho_t(0) + \int_0^{eV}\frac{dT(S,\phi,E,V)}{dV}\rho_s(E)\rho_t(E-eV)\,dE + \int_0^{eV}T(S,\phi,E,V)\rho_s(E)\frac{d\rho_t(E-eV)}{dV}\,dE\Bigg]. \quad (2)$$

It is common in the literature to ignore the latter two terms and use a normalized version of $\frac{dI}{dV}$ as a proxy for the the sample LDOS.[11,21] Even with this simplification, $\rho_s(eV)$ can be calculated only if a good model is available for the tunneling probability $T(S,\phi,E=eV,V)$. This in turn requires knowledge of the tunneling conditions S and ϕ, which are often difficult to directly measure. Furthermore it is easily shown[19,20] that the latter two terms in Eq. (2) can be comparable to the first, and that features in $\rho_t(E)$ directly affect the measured $\frac{dI}{dV}$. Any attempt to solve for $\rho_s(E)$ over a wide bias range should therefore acknowledge these concerns.

Etched tungsten STM tips are preferred for their ease of production and relatively flat tunneling density of states. However, for the present study we are concerned with features in the sample LDOS out to energies of ± 1 eV, and over this range the assumption of constant tip LDOS is poor. Body centered cubic (BCC) tungsten has strongly bonded $5d$ orbitals and the Fermi energy E_F sits in a minimum of the bulk DOS, which has several local maxima in the ± 1 eV range.[22] The analysis is more favorable if we consider only the s- and p-orbital states, which have greater spatial extent and therefore contribute more to the tunneling current. However, even in this case the bulk DOS has a maxima near -0.8 eV.[22] Worse, tungsten tips can exhibit additional features in the s-orbital LDOS, with a maximum near 0.2 eV for BCC pyramids and prominent peaks at 0.2 and -0.8 eV for metastable FCC (face centered cubic) pyramids.[23] Given the uncertainty in the tip condition we choose to focus on extracting the grain-boundary LDOS relative to on-grain LDOS, using the on-grain data to constrain the tip and tunneling conditions (not unlike the comparative scanning tunneling spectroscopy approach discussed in Ref. 19).

The on-grain $\frac{dI}{dV}$ data are typical for tunneling between two metals. If we attribute the difference in measured optical bandgap of AZO compared with undoped ZnO to filling of states in the conduction band, then using 3.37 eV as the bandgap of undoped ZnO we find $E_F - E_c = 0.52 \pm 0.14$ eV. (This estimate is accurate in the absence of band deformation and many-body effects. It is known that for sufficiently high doping levels the bandgap is renormalized downward by $\sim$0.1 eV as the carrier density surpasses the Mott critical density.[30,31] This systematic uncertainty is included in our reported error bounds.) We do in fact observe a dip in the $\frac{dI}{dV}$ data near -0.5 eV [see Fig. 3(b)], but due to uncertainty over the tip LDOS we cannot unambiguously identify this feature with E_c. Instead we use the on-grain $\frac{dI}{dV}$ data to constrain the tunneling parameters and to qualitatively understand the effect of the tip LDOS on the grain-boundary data.

We begin by fitting the on-grain data to the symmetric tunneling probability function introduced by Ukraintsev in Ref. 19. Passoni *et al.* have performed extensive simulations for varying tip and sample LDOS and conclude that the tunneling parameters are best extracted by fitting the positive tail of $\frac{dI}{dV}$ Ref. 24. We therefore measured the on-grain tunneling conductivity out to 1.5 V and fit the tail of this data to extract S and ϕ [Fig. 3(b)]. This approach is bolstered by our understanding of our tip-sample system—at positive bias the sample LDOS is more influential on $\frac{dI}{dV}$ than the tip LDOS, and we are less concerned with unknown electronic features in the tip. At positive energy the on-grain LDOS corresponds to the AZO conduction band, which is known from experiment[25] and theory[26] to be relatively simple (if nonparabolic). It is therefore a reasonable assumption that the positive tail of $\frac{dI}{dV}$ should be free of complicating features. We find that the fit parameters vary little so long as the lower bound of the fit range satisfies $V_{\min} > 0.5$ V. With this lower bound, we find $S = 14.9 \pm 0.3$ Å and $\phi = 4.0 \pm 0.1$ eV, which are reasonable values for tunneling between two metals with nominal work functions near 4.5 eV.[27]

Using the tunneling parameters for the on-grain data, we estimate the parameters for the grain-boundary data in the following manner. Equation (2) can be expressed as a Taylor expansion in powers of V, and the leading term is quadratic. If we assume that the tip and sample LDOS are approximately constant (but not necessarily equal) in a narrow energy range (± 0.05 eV) around E_F, then by comparing the quadratic curvature for grain and grain-boundary data we can relate the tunneling parameters on- and off-grain, with the assumption that the barrier height is constant across the film. We know from independent measurements that the variation in work function across the film is less than 100 meV (see Sec. II and Ref. 21). Variation in ϕ on this scale has negligible impact on the computed results: varying the grain-boundary barrier by ± 0.5 eV changes the calculated S by less then ± 1 Å. With the data normalized so that $dI/dV = 1 + bV^2$ the ratio of the quadratic coefficients $b(\mathrm{GB})/b(\mathrm{GR})$ is equal to 0.55 ± 0.01, where GB and GR indicate grain-boundary and grain, respectively. Finally, from this ratio and the parameters $S(\mathrm{GR}) = 14.9 \pm 0.3$ Å and $\phi(\mathrm{GB}) = \phi(\mathrm{GR}) = 4.0 \pm 0.1$ eV we calculate $S(\mathrm{GB}) = 11.0 \pm 0.4$ Å.

Even with tunneling parameters in hand, extracting the LDOS remains challenging due to the uncertain tip LDOS. Here we follow the approach outlined by Koslowski *et al.* to iteratively solve Eq. (2) for $\rho_s(E)$ under the assumption of constant tip LDOS.[20] This solution begins by using the measured $\frac{dI}{dV}$ normalized to the tunneling probability $T(S,\phi,E = eV,V)$ as an estimate for $\rho_s(E)$. This estimate, which is plotted in Fig. 4(a), shifts the peak at negative energy from -0.65 (in the raw $\frac{dI}{dV}$ data) to -0.76 eV and tends to over-estimate the LDOS for $E - E_F < 0$ due to the asymmetric shape of the tunneling probability function. This estimate is then used to seed a Neumann approximation series that solves Eq. (2) with the third term omitted. This solution is plotted Fig. 4(a). The LDOS peak at negative energy now appears at -0.59 eV. We note that while the LDOS calculated using the average grain-boundary $\frac{dI}{dV}$ now dips below zero for $E - E_F < -0.84$ eV, the upper bound on $\frac{dI}{dV}$ calculated from the scatter in the measured data gives a solution that is strictly positive. As with most STM studies there remains great uncertainty over the scale of the extracted LDOS due to the unknown tip profile. However, in using the on-grain data to constrain the grain-boundary results we can estimate the relative scale of LDOS on- and off-grain. As shown in Fig. 4 the grain-boundary LDOS is on the order of 1% of the on-grain LDOS, which is consistent with our understanding of sputtered AZO films as conducting grains surrounded by insulating grain boundaries.[10,28]

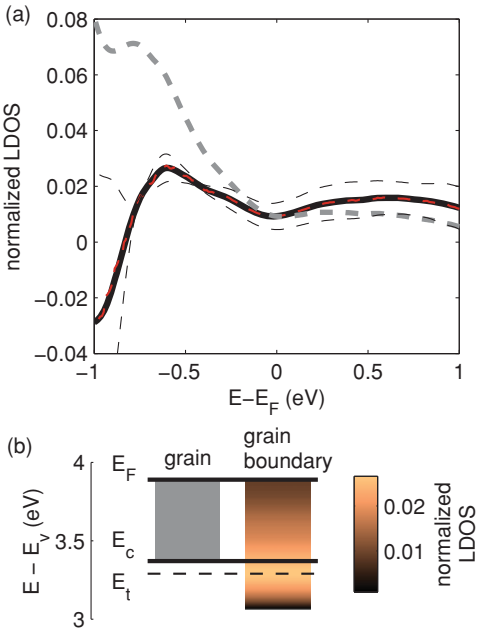

FIG. 4. (Color online) Grain boundary LDOS and electron trap states. (a) Calculated grain boundary LDOS. Data are normalized to the on-grain $\rho_s(E = 0)$ and all calculations are performed using constant tip LDOS. The solid black curve shows the Neumann approximation solution for $\rho_S(E)$, and the dashed black curves show the scatter in the calculated result given the scatter in the raw $\frac{dI}{dV}$ data (see Fig. 3). The dashed red curve shows a simpler solution calculated from a linear combination of $\frac{dI}{dV}$ and $I(V)$ according to Eq. 5 in Ref. 20. These two solutions give nearly identical results. Also shown (grey dashed) is the normalized conductivity $(\frac{dI}{dV})/T$ that is often used as a proxy for the LDOS. A common feature to all solutions is a clear peak at negative $E - E_F$ that represents electron trap states near the conduction band edge. (b) Energy band schematic showing the distribution of grain boundary electron trap states. The degenerately doped conduction band is represented on the left, with $E_F - E_c = 0.52 \pm 0.14$ eV. The spectrum of grain boundary LDOS at negative bias is represented by the colormap using data taken from (a). The trap state density is peaked at $E_t \sim 0.1$ eV below the conduction band edge, E_c.

In quantitative STM analysis the final results are often extraordinarily sensitive to the choice of tip-sample separation. Our analysis largely avoids this complication by constraining the tunneling parameters by both the grain-boundary and on-grain data, and using the calculated LDOS of the latter to normalize that of the former. In this way the sensitivity of our results on tip-sample separation is reduced by a factor of four on a logarithmic scale: e.g., the normalized grain-boundary

LDOS varies by only a factor of ten as the calculated on-grain LDOS varies by a factor of ten thousand for different choices of tip-sample separation. We acknowledge that the on-grain tip-sample separation of 14.9 Å calculated from the data is unphysically large by at least several Å, and that this large value is likely responsible for the calculated grain-boundary LDOS dipping below zero for $E - E_F < -0.84$ eV. However, we emphasize that the results presented in Fig. 4 remain robust on a semiquantitative level, and compared with the alternative of simply assuming a tip-sample separation our comparative analysis technique has the advantage of being constrained by data and explicit in its description.

The broad peak in grain-boundary LDOS centered at $E - E_F \approx -0.6$ eV is naturally associated with the electron trap states that significantly affect electron transport in AZO.[10] The Fermi level lies in the conduction band of our degenerately-doped AZO films, offset from the conduction band edge by $E_F - E_c = 0.52 \pm 0.14$ eV. We conclude that the peak in the grain boundary LDOS lies within the bulk bandgap, ∼100 meV below the conduction band edge, as depicted in Fig. 4(b). The grain boundaries therefore harbor a broad spectrum of electron traps, from shallow states within $\sim k_B T$ of the conduction band edge that may limit electron mobility, to deeper states that may deplete carriers from the the conduction band. We can achieve a very rough estimate of the trap state density in real units by appealing to the theoretical bulk density of states of ZnO Ref. 26, which is calculated to be 0.080×10^{22} cm^{-3}eV^{-1} at $E_F - E_c = 0.52$ eV. At its maximum near −0.6 eV, the trap state LDOS corresponds to 2.2×10^{19} cm^{-3}eV^{-1} in real units. Finally, if we use a unit cell length of 4.2 Å (a rough average of the a and c lattice constants) we obtain an area trap density of states of 9.2×10^{11} cm^{-2}eV^{-1}. This calculation assumes that the grain boundaries are a single unit cell thick. In reality they are likely more than 1 nm in width, in which case our area density needs to be multiplied by a factor of three or more. This calculation, rough as it is, agrees semi-quantitatively with the estimate of 1×10^{13} cm^{-2} for the grain boundary trap density based on transport measurements using a model of trap-limited mobility.[10,28]

IV. CONCLUSION

We have presented an investigation of the electronic structure of granular AZO films using a scanning tunneling microscope. We have measured the electronic structure of the grain boundaries and quantified the electron trap state energy distribution using a variant of comparative scanning tunneling spectroscopy and taking into account much current understanding of STM spectroscopy.[19,20,24] These trap states are broadly distributed in energy and peaked ∼600 meV below the Fermi energy (∼100 meV below the conduction band), suggesting both shallow and deep traps that affect electron transport properties in this important transparent conducting oxide.

ACKNOWLEDGMENTS

This work was supported by NSF/NNIN through the use of their facilities at Harvard University's Center for Nanoscale Systems (CNS). E.M.L. acknowledges support from NSEC. R.J. acknowledges support from the Harvard University Center for the Environment. The authors are thankful for helpful discussion with G. Lengel, T. Williams, W. Hill, and L. Adams.

*rafael@uchicago.edu

[1] U. Ozgur, Y. I. Alivov, C. Liu, A. Teke, M. A. Reshchikov, S. Dodan, V. Avrutin, S.-J. Cho, and H. Morkoc, J. Appl. Phys. **98**, 041301 (2005).
[2] X. D. Wang, C. J. Summers, and Z. L. Wang, Nano Lett. **4**, 423 (2004).
[3] Y. C. Kong, D. P. Yu, B. Zhang, W. Fang, and S. Q. Feng, Appl. Phys. Lett. **78**, 407 (2004).
[4] P. D. Yang, H. Q. Yan, S. Mao, R. Russo, J. Johnson, R. Saykally, N. Morris, J. Pham, R. R. He, and H. J. Choi, Adv. Funct. Mater. **12**, 323 (2002).
[5] R. Cebulla, R. Wendt, and K. Ellmer, J. Appl. Phys. **83**, 1087 (1998).
[6] K. C. Park, D. Y. Ma, and K. H. Kim, Thin Solid Films **305**, 201 (1997).
[7] H. Agura, A. Suzuki, T. Matsushita, T. Aoki, and M. O. M, Thin Solid Films **445**, 263 (2003).
[8] J. Hong, H. Paik, H. Hwang, S. Lee, A. J. deMello, and K. No, Phys. Status Solidi A **206**, 697 (2009).
[9] B. C. Mohanty, H.-R. Choi, and Y. S. Choa, J. Appl. Phys. **106**, 054908 (2009).
[10] K. Ellmer and R. Mientus, Thin Solid Films **516**, 5829 (2008).
[11] F. Matino, L. Persano, V. Arima, D. Pisignano, R. I. R. Blyth, R. Cingolani, and R. Rinaldi, Phys. Rev. B **72**, 085437 (2005).
[12] H. Sato, T. Minami, T. Miyata, S. Takata, and M. Ishii, Thin Solid Films **246**, 65 (1994).
[13] S. Sadewasser, T. Glatzel, S. Schuler, S. Nishiwaki, R. Kaigawa, and M. Lux-Steiner, Thin Solid Films **431**, 257 (2003).
[14] S. Siebentritt, S. Sadewasser, M. Wimmer, C. Leendertz, T. Eisenbarth, and M. Lux-Steiner, Phys. Rev. Lett. **97**, 146601 (2006).
[15] G. Binnig, H. Rohrer, C. Gerber, and E. Weibel, Appl. Phys. Lett. **40**, 178 (1982).
[16] J. Tersoff and D. R. Hamann, Phys. Rev. Lett. **50**, 1998 (1983).
[17] T. E. Feuchtwang, P. H. Cutler, and N. M. Miskovsky, Phys. Lett. A **99**, 167 (1983).
[18] A. P. Roth, J. B. Webb, and D. F. Williams, Phys. Rev. B **25**, 7836 (1982).
[19] V. A. Ukraintsev, Phys. Rev. B **53**, 11176 (1996).
[20] B. Koslowski, C. Dietrich, A. Tschetschetkin, and P. Ziemann, Phys. Rev. B **75**, 035421 (2007).
[21] S. Dasgupta, M. Lukas, K. Dössel, R. Kruk, and H. Hahn, Phys. Rev. B **80**, 085425 (2009).
[22] E. Lassner and W.-D. Schubert, *Tungsten: Properties, Chemistry, Technology of the Element, Alloys, and Chemical Compounds* (Kluwer Academic/Plenum Publishers, 1999).
[23] A. L. Vázquez de Parga, O. S. Hernán, R. Miranda, A. Levy Yeyati, N. Mingo, A. Martín-Rodero, and F. Flores, Phys. Rev. Lett. **80**, 357 (1998).

[24]M. Passoni, F. Donati, A. Li Bassi, C. S. Casari, and C. E. Bottani, Phys. Rev. B **79**, 045404 (2009).
[25]K. Ellmer, J. Phys. D **34**, 3097 (2001).
[26]M. Goano, F. Bertazzi, M. Penna, and E. Bellotti, J. Appl. Phys. **102**, 083709 (2007).
[27]J. M. Pitarke, P. M. Echenique, and F. Flores, Surf. Sci. **217**, 267 (1989).
[28]V. Srikant, V. Sergo, and D. R. Clarke, J. Am. Ceram. Soc. **78**, 1935 (1995).
[29]J. A. Stroscio, R. M. Feenstra, and A. P. Fein, Phys. Rev. Lett. **57**, 2579 (1986).
[30]B. E. Sernelius, K.-F. Berggren, Z.-C. Jin, I. Hamberg, and C. G. Granqvist, Phys. Rev. B **37**, 10244 (1988).
[31]J. J. Lu *et al.*, J. Appl. Phys. **101**, 083705 (2007).